https://doi.org/10.5194/nhess-2019-166
Preprint. Discussion started: 1 August 2019

Natural Hazards and Earth System Sciences
Discussions

Evaluation of the probable annual flood damage influenced by El-Niño in the Kan River Basin, Iran

Farhad Hooshyaripor[1], Sanaz Faraji-Ashkavar[2], Farshad Koohyian[3], Qiuhong Tang[4,5*], Roohollah Noori[6]

[1]Department of Civil Engineering, Architecture and Art, Science and Research Branch, Islamic Azad University, Tehran, 1477893855, Iran
[2]Department of Civil Engineering, Al-Taha University, Tehran, 1488836164, Iran
[3]Water Research Institute, Ministry of Energy, Tehran, 1658954381, Iran
[4]Key Laboratory of Water Cycle and Related Land Surface Processes, Institute of Geographic Sciences and Natural Resources Research, Chinese Academy of Sciences, Beijing, 100101, China
[5]University of Chinese Academy of Sciences, Beijing, 100049, China
[6]School of Environment, College of Engineering, University of Tehran, Tehran, 141785311, Iran

Correspondence to: Qiuhong Tang (tangqh@igsnrr.ac.cn)

Abstract. Although many studies have explored the effect of teleconnection indicators on flood, few investigations have focused on the assessment of the expected damages resulted by flood under the El-Niño or La-Niña condition. Therefore, this study's aim was to determine the effect of El-Niño on the expected flood damage in the Kan River basin, Iran. To determine the flood damage costs, first, the precipitation enhancement during El-Niño condition was estimated then using a probabilistic approach the inundation area was determined under 5, 10 and 50 year return periods. The results showed that El-Niño increases the precipitation amount up to 8.2% and 31% with 60% and 90% confidence level, respectively. Flood damage assessment using damage-elevation curves showed that the expected increase percentile in flood damage for smaller return periods, which is more frequent, is much more than that for larger return periods. In general, for the return periods of 5- and 10- year, 31% increase in the precipitation would result in 2416% and 239% damage increase, respectively. However, for the 50-year rainfall this increase amount will be about 74%. These results indicate the importance of small flood events in flood management planning during El-Niño.

1 Introduction

In recent decades, the frequency of flood events and the resultant damages have been increased dramatically in Iran. Reviewing the recorded flood events in the past decades shows an increasing trend. According to the available reports, the number of flood events in Tehran over four decades from 12 cases in 1951 reached to 54 cases in 1991 (Saghafian et al. 2017). Climate change, approaching to floodplain, land use changes, diversion of the waterways, population increase and destructive effects of human activities, degradation of forests and pastures, construction of dysfunctional and vulnerable hydraulic structures can be mentioned as the reasons for increasing flood risks.

https://doi.org/10.5194/nhess-2019-166
Preprint. Discussion started: 1 August 2019


Natural Hazards and Earth System Sciences Discussions

The magnitude and frequency of flood events in each region depends on several factors: (i) physiographical features of the catchment such as shape, slope, and rivers network density, (ii) hydrological features such as precipitation, storage and initial losses, evapotranspiration, and permeability, (iii) human activities, (iv) large-scale atmospheric signals and (v) climate change. These factors affect the occurrence frequency and intensity of the flood and consequently the amount of damage costs. Identifying these factors will help to manage the flood and reduce the risks. In recent years, the effects of teleconnection phenomena have been more and more discussed and has tried to identify their impact on the local climate (Ward et al. 2014; Saghafian et al. 2017; Hooshyaripor et al. 2018; Hao et al. 2018; Canedo-Rosso et al. 2019).

Prediction of teleconnection indicators helps to reduce the flood damages by predicting the necessary measures (Schöngart and Junk 2007). Sun et al. (2015) showed that parts of North and South America, South and East Asia, South Africa, Australia and Europe are affected by El-Niño Southern Oscillation (ENSO). Research of Träger-Chatterjee et al. (2013) in Germany and adjacent areas showed that if ENSO is not very intensely developed, extremely high solar irradiation and low precipitation amounts during late winter/spring and extremely sunny and dry summer months would be expected. Grieco and DeGaetano (2018) concluded that the occurrence of El-Niño in the winter reduces the frequency of high waves in the east of the Ontario Lake, while there was no meaningful relationship in the conditions of La-Niña. Azmoodehfar and Azarmsa (2013) showed that the south-east of Iran during the years with the event of La-Niña experienced a higher-than-normal maximum and minimum temperature. It has been proven that during El Niño years, a significant decrease in crop yields followed by a severe drought can be expected in Bolivian Altiplano (Canedo-Rosso et al. 2019). Hooshyaripor et al. (2018) investigated the impact of different teleconnection indices on Iran rainfall, and concluded that El-Niño can enhance the annual precipitation by nearly 40% in some regions. They stated that due to the increase of rainfall, the river discharge will be affected directly. So far, many studies have focused on the impact of El-Niño over river flow. Schöngart and Junk (2007) showed that there is a strong correlation between ENSO and Amazon River flood such that the river water level decreases in the warm episode of the ENSO (El-Niño) and increases in its cold episode (La-Niña). In a global study, Ward et al. (2014) studied the impact of ENSO on the daily peak discharge of some important rivers.

These studies indicate the importance of teleconnection in the flood characteristics in many parts of the world. To the best of the authors' knowledge few investigations have focused on the assessment of the expected damages under the El-Niño or La-Niña condition. Obviously, damage assessment is an important part of the flood risk analysis, which determines the need for flood management programs and their priorities. The question responded in this research is that, given the increasing impact of rainfall due to El-Niño, how much losses/damages is expected to be added in a specified study area. To answer this question, the catchment of Kan River in north of Tehran metropolis was selected.

2 Study area

Kan River basin is one of the most important flooding basins located in the north of Tehran city and a vulnerable area against flood (WRI 2011a; Yazdi and Salehi Neyshabouri 2012; Yazdi et al. 2013). It is reported that in the flood of July 15, 2015 a

https://doi.org/10.5194/nhess-2019-166
Preprint. Discussion started: 1 August 2019

Natural Hazards and Earth System Sciences Discussions

20-minute storm caused 8 losses of life, several bridge and diversion dam failures, and more than 10 million dollars in damages to the residential, commercial and agricultural areas. In June 1968 a heavy rain spouted 6 times of the annual precipitation in 2 days had caused 31 losses of life in Tehran central area and huge damage to the properties. In general, during a period of 60-year (from 1954 to 2015) at least 8 flood evens resulted in loss of life (in total 2200 people) have been reported in Kan and central Tehran areas. Existence of many restaurants, demographic, recreational, tourist and pilgrimage centers adjacent to the sloping Kan River have exacerbated the potential for damage (WRI 2011a).

The Kan basin is located between the longitude of the 51 °10' and the 51 °23' and the latitude of 35 °45' to 35 °58'. The basin can be divided into 10 sub-basins. The highest point of the basin is 3823 m and the lowest point is 1328 m with the average of 2377 m above sea level. The area of the basin is 216 km^2. The average annual precipitation is 640 mm and the average annual discharge is 78.23 Mm^3 at Sulaghan station. The hydrometric stations include Kiga (Gage 1), Keshar (Gage 2) and Sulaghan (Gage 3) (Fig. 1). As shown in Fig 1 three rain gage stations in the basin and four synoptic stations around the basin record the precipitation.

3 Methodology and data

According to the previous study ENSO is the most important large-scale atmospheric signal that affects Iran's climate (Hooshyaripor et al. 2018). It has been shown that rainfall intensity increases in the conditions of El-Niño and decreases in the conditions of La-Niña. Accordingly, the present study will assess the increase in flood damage due to El-Niño occurrence. For this purpose, the following steps have been taken.

Step I: Estimating the lag time (T_l) between the El-Niño event and the precipitation in the study area. Doing so, the monthly rainfall at the nearby synoptic stations of Mehrabad (1951-2017), Shemiran (1988-2017), Tehran-Geophysics (1992-2017) and Chitgar (1997-2017) are used (See Fig. 1).

For this, the average mutual information (AMI) method is used. This method is based on the Shannon entropy theory and is a measure of the "amount of information" obtained about one random variable, through the other random variable. Suppose A is monthly precipitation in the representative station of the basin and B is the Southern Oscillation Index (SOI). The AMI is defined between two measurements a_i and b_i belonging to the sets A and B, respectively as follows (Cover and Thomas 1991):

$$I_{AB} = \sum_{i=1}^{K}\sum_{j=1}^{K} P_{AB}\left(a_i, b_j\right)\log\left(\frac{P_{AB}\left(a_i, b_j\right)}{P_A\left(a_i\right)P_B\left(b_j\right)}\right) \quad (1)$$

where $P_{AB}(a_i, b_j)$ is the conjugate probability density for measurements A and B with values of a and b, respectively; $P_A(a_i)$ and $P_B(b_j)$ are the probability density function for measurements A and B.

If a_i (the measurements of A) is independent of b_i (the measurements of B) then the value of I_{AB} will be zero. This method determines the lag time between two-time series by using the nature of the data itself and without any predetermined format

https://doi.org/10.5194/nhess-2019-166
Preprint. Discussion started: 1 August 2019

Natural Hazards and Earth System Sciences Discussions

based on probabilistic concepts (Cover and Thomas 1991). In Eq. (1), K is the optimal number of statistical categories for fitting the statistical distribution on the measurements A and B which can be calculated from Eq. (2):

$$K = 1+3.322 \log (n) \quad (2)$$

where n is the number of data in the corresponding interval (here n = 480); therefore, in the present study, K = 10.

Step II: Estimating the amount of rainfall variation under the influence of El-Niño: In this step, the SOI is applied. It is a standardized index based on the observed sea level pressure differences between Tahiti and Darwin. In this study SOI values were obtained from National Oceanic and Atmospheric Administration (NOAA) website (https://www.cpc.ncep.noaa.gov/data/indices/soi). Prolonged periods of negative SOI values accompany the abnormally warm ocean waters across the eastern tropical Pacific. In months with SOI value of more than +0.8, La-Niña and months with an index of less than -0.8, El-Niño are occurred, and in the other cases we have normal conditions (Australia Bureau of meteorology 2012). Then, the average precipitation change in the El-Niño condition (ΔP) is calculated as follow:

$$\Delta P = \frac{\sum_{i=1}^{n} \left(P_{El\,i} - P_N\right)/P_N}{n} \times 100 \quad (3)$$

where P_{El} is the annual rainfall in the El-Niño episode; P_N average annual rainfall in the normal episodes; and n is number of El-Niño episodes in the time period.

Step III. Estimation of rainfall design with different return periods: The intensity-duration-frequency (IDF) rainfall curve of Kan basin is obtained from Water Research Institute (WRI 2011b). The time of concentration of the basin is T_c=135.19 min (Using Kirpich equation). Therefore, the intensity of the design rainfall can be deduced for different return periods. In this research, three return periods of 10, 25 and 50 years are considered for the rainfall storms. As the El-Nino affects the rainfall intensity, then three distinct scenarios of El-Niño influence (normal, weak El-Niño and strong El-Niño conditions) were defined and every rainfall return period was examined in the scenarios. Therefore, totally 9 different models were evaluated here. The scenarios are:

- Scenario I (normal condition): In the first scenario no El-Niño event is considered. It is assumed that the basin receives a natural uniform rainfall with the given intensities (T=10, 25, and 50) in T_c min duration.
- Scenario II (weak El-Niño condition): In the second Scenario it is assumed that a T_c min rainfall with the increased intensity affected from El-Niño by 60% probability reaches to the basin, uniformly.
- Scenario III (strong El-Niño condition): In the second it is assumed that a T_c min rainfall with the increased intensity affected from El-Niño by 90% probability reaches to the basin, uniformly.

Step IV: Hydrological modeling: As the design rainfall is determined, the HEC-HMS model is used to simulate the rainfall-runoff process. The SCS method is used to calculate the effective rainfall (P_e):

https://doi.org/10.5194/nhess-2019-166
Preprint. Discussion started: 1 August 2019


Natural Hazards and Earth System Sciences Discussions

$$P_e = \frac{(P - 0.2S)^2}{P + 0.8S} \quad (4)$$

where P is rainfall; and S is storage potential. Moreover, Clark instantaneous unit hydrograph method is applied to transform the effective rainfall into runoff (Q). Two-parameter Muskingum method is used for flood routing. The Muskingum method calculates the discharge within the river given the inflow hydrograph at the upstream end. For calibration of the HEC-HMS model, hourly historical storms which had been recorded in 3 rain gage stations in the basin and the related runoffs at the hydrometric stations (Fig. 1) are used and the curve numbers (CN) and time of concentrations (T_c) are calibrated within the 10 sub-basins. For calibration and verification of the hydrologic model two largest storm events were extracted from 15 years available data (2000-2014): the first is the storm of 15–18 April 2003 in which a flood of maximum 38.22 m^3/s was recorded at Gage3 and the second event is the storm of 16–19 April 2002 where the peak discharge rate of 32.3 m3/s was recorded at Gage3. Then the calibrated model can be used for modelling the rainfall of given return periods to calculate the flood hydrographs at the outlet of the sub-basins.

Step V: Hydraulic modeling: the HEC-RAS model is used for hydraulic modeling and determination of flow depth and velocity at the target points (Residential areas shown in Fig. 1). HEC-RAS is a one-dimensional model based on the numerical solution of the Saint-Venant equations. The model calibration is done by adjusting the Manning roughness coefficients at different river sections. The calibrated model then is used under steady state condition to model the obtained peak discharges from HEC-HMS in order to calculate flood depths at the target points.

Step VI. Estimating expected damage cost: Damage caused by flooding can be divided into two groups: tangible and intangible damages. Intangible damages are those caused by illnesses and mental problems due to loss of life or properties. Tangible damage can be categorized into two direct and indirect damages. Direct damage is that caused from flooding of the buildings and properties such as home equipment, crops, livestock and poultry. Indirect damages are those caused due to disruption of trade and business, threating life and needs to emergency services, and so on. Noted that, this paper focuses on the direct tangible damages only.

Damage caused by flood is a function of its characteristics, including flow depth and inundation amount, time of inundation, and flow velocity. One of the commonly used methods for estimating flood damages is damage-elevation curve method which gives the relationship between damage percentile and flood depth (Corry et al. 1980, Messner et al. 2007; Olesen et al. 2017; Wobus et al. 2017; Jamali et l. 2018). They are prepared for different land uses of the Kan river basin (WRI 2011a; Yazdi et al. 2013). This method has been developed by the Federal Emergency Management Administration (Berkman and Brown 2015). The main land uses of the Kan River floodplain are residential buildings, restaurants, and fruit gardens (WRI 2011a). The damage cost then is calculated having entire monetary value of the inundated land uses.

https://doi.org/10.5194/nhess-2019-166
Preprint. Discussion started: 1 August 2019

Natural Hazards and Earth System Sciences Discussions

4 Results and discussion

Monthly analyses of the precipitation in the synoptic stations and SOI using AMI method showed that there is no lag time between rainfall and SOI time series (the lag time is less than one month).

In Fig. 2, the annual rainfall of stations is plotted against the SOI index. It is obvious that with decreasing SOI index, annual rainfall increases in the study area and vice versa. In the period of 1950 to 2017, a total of 9 El-Niño (SOI<-0.8) and 7 La-Niña (SOI>+0.8) events have been occurred. The largest event for El-Niño dates back to 1983 and 1987 with respectively 334 mm and 252 mm recorded rainfall in Mehrabad station. According to the long lifetime of Mehrabad station and its sufficient data compared to the other stations, Mehrabad station is used for the further analyses.

Evaluation of the values of SOI over the period from 1952 to 2017 shows that 197 months with El-Niño, 163 months with La-Niña, and 432 normal months have been occurred. The average rainfall at Mehrabad station in the months of El-Niño is 22.2 mm and in the months of La-Niña 16.96mm, while in the normal months, the average rainfall is 18.41 mm. Therefore, using Eq. (3) El-Niño increases the rainfall amount in the study area by 20.6% and La-Niña decreases it by 7.86%.

In the risk analysis, it is required to evaluate the annual damage costs. There are 9 years with El-Niño and 7 years with La-Niña condition in the total of 66 years. Therefore, using Eq. (3) the annual increased percentiles of rainfall in the El-Niño years can be calculated. Then a probability distribution can fit on these percentiles for further probabilistic analysis. Figure 3 illustrates the cumulative distribution function fitted on the annual increased percentiles of rainfall. On the basis of Kolmogorov-Smirnov goodness of fit method, Gumbel distribution can be fitted well on the data in 99% confidence interval. According to Fig. 3, it can be said that by 90% and 60% certainty the increased percentiles of rainfall during El-Niño years is less than 31% and 8.2% respectively compared to the normal years.

Noted, the most historical increase in annual rainfall is related to the year 1983 with 42.6% amount increase in which 334 mm rainfall has been recorded. Based on these results, three scenarios of increase rate of rainfall are investigated. In the first scenario (normal condition) rainfall is assumed to occur in the normal condition without any increase in the rainfall amount. In the second scenario (weak El-Niño condition), rainfall is assumed to increase by 8.2% (60% confidence interval), and in the third scenario (strong El-Niño effect), an increase of 31% rainfall is supposed to be taken place due to El-Niño (90% confidence interval).

The Kan River basin has 135.19 min time of concentration. Therefore, considering the duration of the design rainfall as D=150 min, the rainfall intensity (i_d) can be estimated from IDF curves. For return periods of 5, 25, and 50-yr, i_d values are 7.8, 9.5, and 13 mm/hr, respectively. Thus, in the first scenario, three storms with the abovementioned intensities during D=150 min are modeled. In the second and third scenarios it is assumed that with the same duration, total rainfalls increased by 8.2% and 31%, respectively.

https://doi.org/10.5194/nhess-2019-166
Preprint. Discussion started: 1 August 2019


Natural Hazards and Earth System Sciences Discussions

4.1 Hydrologic and hydraulic modeling

HEC-HMS is calibrated using an actual rainfall and runoff event recorded in April 2003. The calibration parameters include curve number and concentration time (T_c) of the sub-basins. In the process of automatic calibration, the parameters are determined such a way that the model could simulate the hydrologic behaviour of the basin accurately. The main objective is to predict the exact peak discharge and time to peak of the hydrograph in the hydrometric stations by minimizing the mean squared error (MSE) between predicts and observations (Fig. 4a). In Table 1, the calibration result of the hydrologic model is presented. Then the hydrologic model is verified with the storm event in April 2002 (Fig. 4b) and finally used for modelling the design storms in the three scenarios to calculate the flood hydrographs at the sub-basins.

Then HEC-RAS software is used to simulate the flood travelling and to determine the flood depths of different return periods in the target points. For the model's calibration, the peak discharges produced in the hydrologic model's calibration step (flood 15–18 April 2003) are input into the hydraulic model as the boundary conditions at the upstream reaches and the flood depth and discharge at Sulaghan station is compared with the observed one. The calibration parameters are Manning roughness coefficients that are calibrated manually. For the model verification, flood in 16–19 April 2002 and the upstream peak discharges generated in the hydrologic model are used.

Therefore, the hydraulic model can be used for calculating the flow depth at the target points. The hydrologic and hydraulic models are applied for modelling the design storms of different 5, 25, and 50 return periods under three defined scenarios. It means that totally 9 different runs of the sequent models are required. Using the obtained inundated depths, the flood mapping can be done in ArcMAP. Figure 5 illustrates the inundation areas at two target points (Sulaghan and Sangan villages) for the 50-yr flood in the first scenario.

4.2 Damage analysis

In this section, with the help of GIS tool and the land use maps which were obtained from the local municipality, a comprehensive analysis of damages to the buildings and their contents is carried out. In this step just five Sub-basins of Imamzadeh Davood, Rendan, Sangan, Sulaghan and Keshar are considered; because of lack of land use maps, low population, and low development in the other sub-basins. For this regard, flood zoning maps are first used to calculate the average depth of land uses' inundation. Based on the average flooding depth and the damage-elevation curves, percentile of damage to the land uses can be estimated. The damage cost to each of land uses is calculated by the average economic value of one unit of that land use. It should be noted that the average value of different assets in the flooding area is obtained by a field survey and interviews with the local authorities. Table 2 provides the details of the physical damage costs to the present land uses for the 50-year flood. Similarly, two scenarios of rainfall increase are simulated and the damages are estimated in the same procedure. Table 3 shows the amount of flood damages cost for different return periods in the three considered scenarios. This table revealed that, firstly, the expected flood damages cost during El-Niño event increases much more than that of rainfall increase, and secondly, in the smaller return periods, the increases of flood damages is much more than that in the bigger return periods.

https://doi.org/10.5194/nhess-2019-166
Preprint. Discussion started: 1 August 2019


Natural Hazards and Earth System Sciences Discussions

In the return period of 5-year, with 60% probability El-Niño may increase the damages up to 1072%, although the expected increase for the rainfall is 8.2%. Also, with 90% probability the increased damages cost is less than 2959% compared to the normal condition. The main reason for this high amount is that the average depth of 5-yr flood is very small (<0.04m) and with an increase of 8.2% or 31% in the rainfall amount, the flood depth increases considerably (respectively less than 0.41m and 0.63m). During the 10-yr flood, due to El-Niño, increases up to 133% (by 60% probability) and 289% (by 90% probability) are expected to be seen in the flood damages cost. Similarly, for the return period of 50-year, the increase in the probable flood losses would drop to 41% and 74% at the probability level of 60% and 90%, respectively.

5 Conclusions

In the present paper, the effect of El-Niño on the probable flood damages was investigated. The methodology was based on the calculation of increasing rainfall amount at 60% and 90% confidence intervals during El-Niño event compared to the normal conditions. The increase percentile of the rainfall was then applied for generating design storms of different return periods of 5, 10 and 50 years. Here, three scenarios were defined: 1) normal condition scenario; 2) rainfall increase scenario because of El-Niño at 60% confidence level (equal to 8.2% increase in the rainfall intensity); and 3) rainfall increase scenario at 90% confidence level (31% increase in the rainfall intensity due to El-Niño). Using HEC-HMS and HEC-RAS models flood zoning was performed in the three defined scenarios and three return periods, as well. Therefore, a total of 9 models were developed and flood zoning results turned into physical damage. To estimate the flood damage cost the damage-elevation curve method was used. The results showed that the occurrence of El-Niño in less return periods, which is more frequent, increases the damages very much and for the higher return periods the increase percentile drops considerably. More specifically in a flood with a return period of 5 years, with a 90% chance an increase of 2959% may be occurred. The average increase in the expected damages cost is 1072% for 5-yr return period, while it is 133% and 41% for 10-yr and 50-yr return periods, respectively. It is remarkable that rainfall intensity increases by 8.2% and 31% in the second and third scenarios. Consequently, it implies that the flood management in this basin should pay more attention to the small floods during the El-Niño years. In general, flood management in small flood case requires much less financial budget and may result in much more effective approaches.

Acknowledgments

This research is partially supported by the National Natural Science Foundation of China (41790424, 41730645, 41425002), the Strategic Priority Research Program of the Chinese Academy of Sciences (XDA20060402), and the International Partnership Program of Chinese Academy of Sciences (131A11KYSB20170113). Qiuhong Tang is supported by the Newton Advanced Fellowship.

https://doi.org/10.5194/nhess-2019-166
Preprint. Discussion started: 1 August 2019

Natural Hazards and Earth System Sciences Discussions

Conflict of interest

The authors declare no conflict of interest.

References

Australia Bureau of Meteorology: Record-breaking La Niña events An analysis of the La Niña life cycle and the impacts and significance of the 2010–11 and 2011–12 La Niña events in Australia, Bureau of Meteorology, July 2012.

Azmoodehfar, M.H. and Azarmsa, S.A.: Assessment the Effect of ENSO on Weather Temperature Changes Using Fuzzy Analysis (Case Study: Chabahar). APCBEE Procedia, 5, 508-513, 2013.

Berkman, M.P. and Brown, T.: Estimating Flood Impacts: A Status Report, pp. 15 - 18, Auckland, New Zealand, 2015.

Canedo-Rosso, C., Hochrainer-Stigler, S., Pflug, G., Condori, B., and Berndtsson, R.: Drought risk in the Bolivian Altiplano associated with El Niño Southern Oscillation using satellite imagery data, Nat. Hazards Earth Syst. Sci. Discuss., https://doi.org/10.5194/nhess-2018-403, in review, 2019.

Corry, M., Jones, J. and Thompson, D.: The design of encroachments of floodplains using risk analysis, Hydraulic Engineering Circular, No. 17, Department of Transportation, Federal Highway Administration, Washington, DC, 1980.

Cover, T.M. and Thomas, J.A.: Elements of Information Theory (Wiley ed.). ISBN 978-0-471-24195-9, 1991.

Grieco, M.B. and DeGaetano, A.T.: A climatology of extreme wave height events impacting eastern Lake Ontario shorelines. Theoretical and Applied Climatology, 136(1-2), 543-552, 2019.

Hao, Z., Hao, F., Singh, V.P., Zhang, X.: Quantifying the relationship between compound dry and hot events and El Niño–Southern Oscillation (ENSO) at the global scale, Journal of Hydrology, 567, 332-338, 2018.

Hooshyaripor, F., Faraji Ashkour, S., Koohian-Afzal, F. and Dehghani, M.: Estimation of the Effect of Large-Scale Signals on Regional Rainfall of Iran by Statistical Analysis. Asas Journal, 20(53), 65-76, 2018 (In Persian).

Jamali, B., Löwe, R., Bach, P.M., Urich, C., Arnbjerg-Nielsen, K., Deletic, A.: A Rapid Urban Flood Inundation and Damage Assessment Model, Journal of Hydrology 564, 1085-1098, doi: https://doi.org/10.1016/ j.jhydrol.2018.07.064, 2018

Messner, F., Penning-Rowsell, E., Green, C., Meyer, V., Tunstall, S. and Veen, D: Evaluating flood damages: guidance and recommendations on principles and models, Sixth framework programme for European research and technological development, integrated project flood site, Document Reference T09-06-01, 2007.

NOAA, http://www.cpc.ncep.noaa.gov/data/indices/soi, 2018.

Olesen, L., Löwe, R., Arnbjerg-Nielsen, K.: Flood Damage Assessment Literature Review and Recommended Procedure, Cooperative Research Centre for Water Sensitive Cities, Melbourne, Australia, 2017.

Saghafian, B., Haghnegahdar, A. and Dehghani, M.: Effect of ENSO on annual maximum floods and volume over threshold in the southwestern region of Iran. Hydrological Sciences Journal, 62(7), 1039-1049, 2017.

Schöngart, J. and Junk, W.J.: Forecasting the flood-pulse in Central Amazonia by ENSO-indices. Journal of Hydrology, 335(1), 124-132, 2007.

https://doi.org/10.5194/nhess-2019-166
Preprint. Discussion started: 1 August 2019

Sun, X., Renard, B., Thyer, M., Westra, S. and Lang, M.: A global analysis of the asymmetric effect of ENSO on extreme precipitation. Journal of Hydrology, 530, 51-65, 2015.

Träger-Chatterjee, C., Müller, R. W., and Bendix, J.: Analysis of extreme summers and prior late winter/spring conditions in central Europe, Nat. Hazards Earth Syst. Sci., 13, 1243-1257, https://doi.org/10.5194/nhess-13-1243-2013, 2013.

Ward, P.J., Eisner, S., Florke, M., Dettinger, M.D. and Kummu, M.: Annual flood sensitivities to El Nino-Southern Oscillation at the global scale. Hydrol. Earth Syst. Sci., 18, 47-66, 2014.

Wobus, C., Gutmann, E., Jones, R., Rissing, M., Mizukami, N., Lorie, M., Mahoney, H., Wood, A. W., Mills, D., and Martinich, J.: Climate change impacts on flood risk and asset damages within mapped 100-year floodplains of the contiguous United States, Nat. Hazards Earth Syst. Sci., 17, 2199-2211, 2017.

WRI: Integrated flood management, case study: Kan basin. Report of flood vulnerability assessment, Water Research Institute, Ministry of Energy, Iran, 2011a.

WRI: Integrated flood management, case study: Kan basin, Report of Hydrologic Study and Flood, Water Research Institute, Ministry of Energy, Iran, 2011b.

Yazdi, J. and Salehi Neyshabouri, S.A.A.: Optimal design of flood-control multi-reservoir system on a watershed scale. Natural Hazards, 63(2), 629–646, 2012.

Yazdi, J., Salehi Neyshabouri, S.A.A., Niksokhan, M.H., Sheshangosht, S. and Elmi, M.: Optimal prioritisation of watershed management measures for flood risk mitigation on a watershed scale. Journal of Flood Risk Management, 6(4), 372-384, 2013.

https://doi.org/10.5194/nhess-2019-166
Preprint. Discussion started: 1 August 2019

Natural Hazards and Earth System Sciences
Discussions

Table Captions:

Table 1: Calibration results of the hydrologic model

Table 2: Physical damages to the sub basins properties for 50-yr flood in different scenarios

Table 3: Flood damages cost and expected increases during El-Niño event

https://doi.org/10.5194/nhess-2019-166
Preprint. Discussion started: 1 August 2019

Natural Hazards and Earth System Sciences
Discussions

Figure Captions:

Figure 1: Location of Kan River Basin in north of Tehran plain, Iran

Figure 2: Annual rainfall against SOI index in the station of a) Mehrabad, b) Shemiran, c) Chitgar and 4) Tehran Geophysics

Figure 3: Gumbel Cumulative distribution function fitted on the annual increased percentiles of rainfall

Figure 4: The observed and simulated flood hydrographs at Sulaghan Station in a) calibration step (15–18 April 2003) and b) verification step (16–19 April 2002)

Figure 5: The 50yr floodplain in the sub-basins of a) Sulaghan and b) Sangan

https://doi.org/10.5194/nhess-2019-166
Preprint. Discussion started: 1 August 2019

Natural Hazards and Earth System Sciences
Discussions

Table 1- Calibration results of the hydrologic model

No.	Sub-basin	Area (km^2)	Calibration parameter	
			CN	*Tc* (hr)
1	Imamzadeh Davood	23.77	71.87	1.05
2	Rendan	33.61	72.35	0.874
3	Sangan	47.43	71.37	1.227
4	Taloon	26.65	71.39	0.932
5	Kiga	4.40	70.2	0.332
6	Doab	7.19	71.71	0.511
7	Keshar	34.85	71.83	1.181
8	Herias	11.44	70.7	0.759
9	Sulaghan	13.66	71.1	0.556
10	Jangalak	12.89	71.9	0.623

https://doi.org/10.5194/nhess-2019-166
Preprint. Discussion started: 1 August 2019

Natural Hazards and Earth System Sciences Discussions

Table 2- Physical damages to the sub basins properties for 50-yr flood in different scenarios

First scenario					
Sub-basin	Average inundation depth (m)	Damage to residential building (10^3US$)	Damage to content (10^3US$)	Damage to restaurant (10^3US$)	Damage to agriculture (US$)
Imamzadeh Davood	0.61	201	37	42	519
Rendan	0.6	68	12	20	723
Sangan	0.5	393	68,084	19	1,259
Keshar	0.66	343	62	67	550
Sulaghan	0.25	81	11	55	843
Sum (10^3US$)		**1,086**	**190**	**203**	**3,893**
Total damage cost (10^3US$)					**5,372**
Second scenario					
Imamzadeh Davood	0.76	246	49	51	715
Rendan	0.7	816	15	24	935
Sangan	0.66	455	82	22	2,098
Keshar	0.82	483	92	95	715
Sulaghan	0.45	176	40	119	1,080
Sum (10^3US$)		**1,441**	**277**	**311**	**5,543**
Total damage cost (10^3US$)					**7,572**
Third scenario					
Imamzadeh Davood	0.89	324	61	67	832
Rendan	0.79	88	18	26	1,028
Sangan	0.76	517	102	25	2,398
Keshar	0.89	514	98	101	739
Sulaghan	0.65	298,	54	201	1,844
Sum (10^3US$)		**1,741**	**333**	**421**	**6,840**
Total damage cost (10^3US$)					**9,334**

https://doi.org/10.5194/nhess-2019-166
Preprint. Discussion started: 1 August 2019

Natural Hazards and Earth System Sciences
Discussions

Table 3- Flood damages cost and expected increases during El-Niño event

T (yr)	Damage cost (US$)			Damage increase (%)	
	1th scenario (no El-Niño effect)	2nd scenario (8.2% rainfall increase)	3rd scenario (31% rainfall increase)	2nd scenario	3rd scenario
5	120,529	1,413,100	3,032,458	1,072	2,416
10	1,393,753	3,256,633	5,149,147	133	269
50	5,372,472	7,571,796	9,334,019	41	74

https://doi.org/10.5194/nhess-2019-166
Preprint. Discussion started: 1 August 2019

Natural Hazards and Earth System Sciences
Discussions
Open Access
EGU

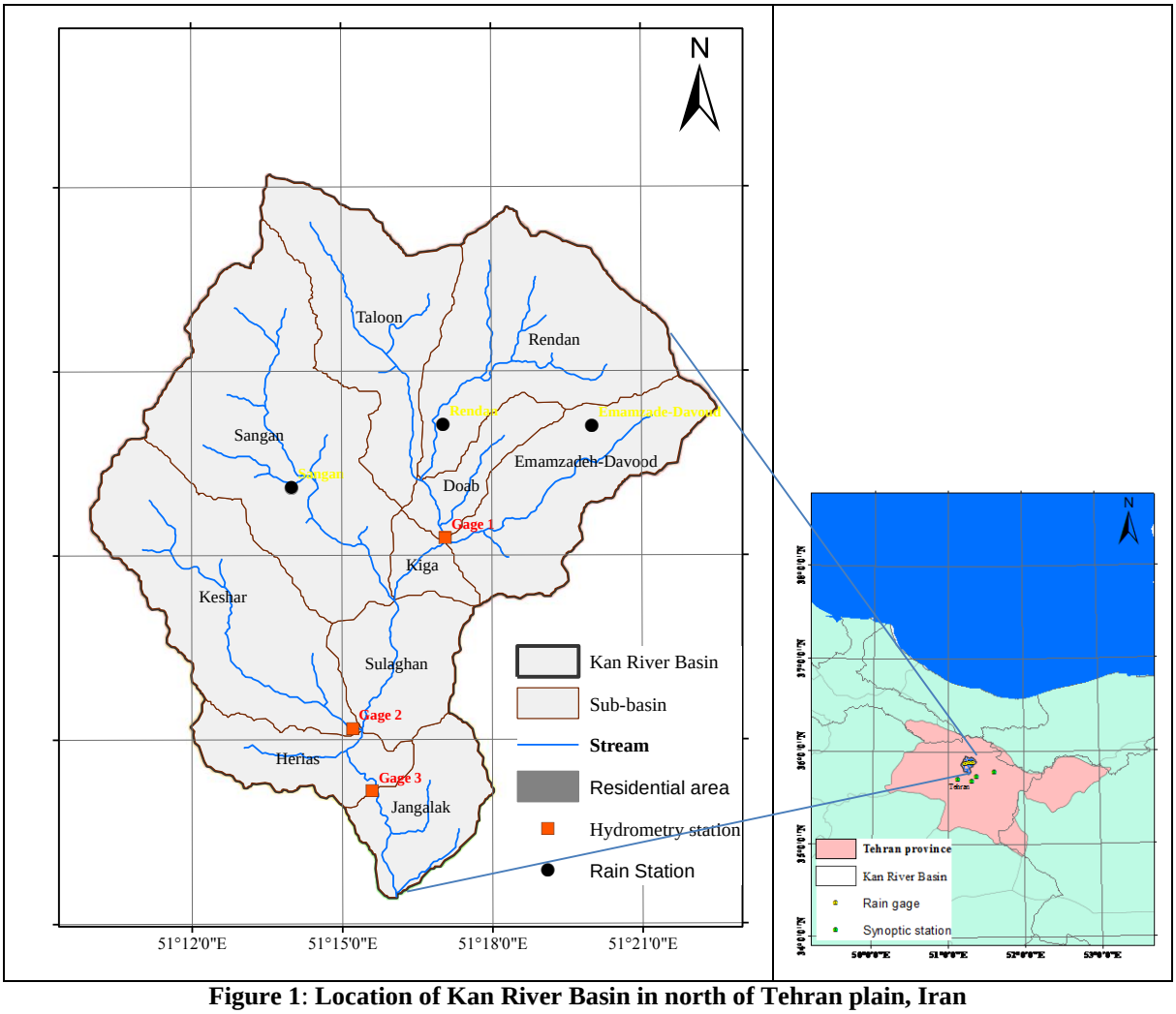

Figure 1: **Location of Kan River Basin in north of Tehran plain, Iran**

https://doi.org/10.5194/nhess-2019-166
Preprint. Discussion started: 1 August 2019

Natural Hazards and Earth System Sciences
Discussions

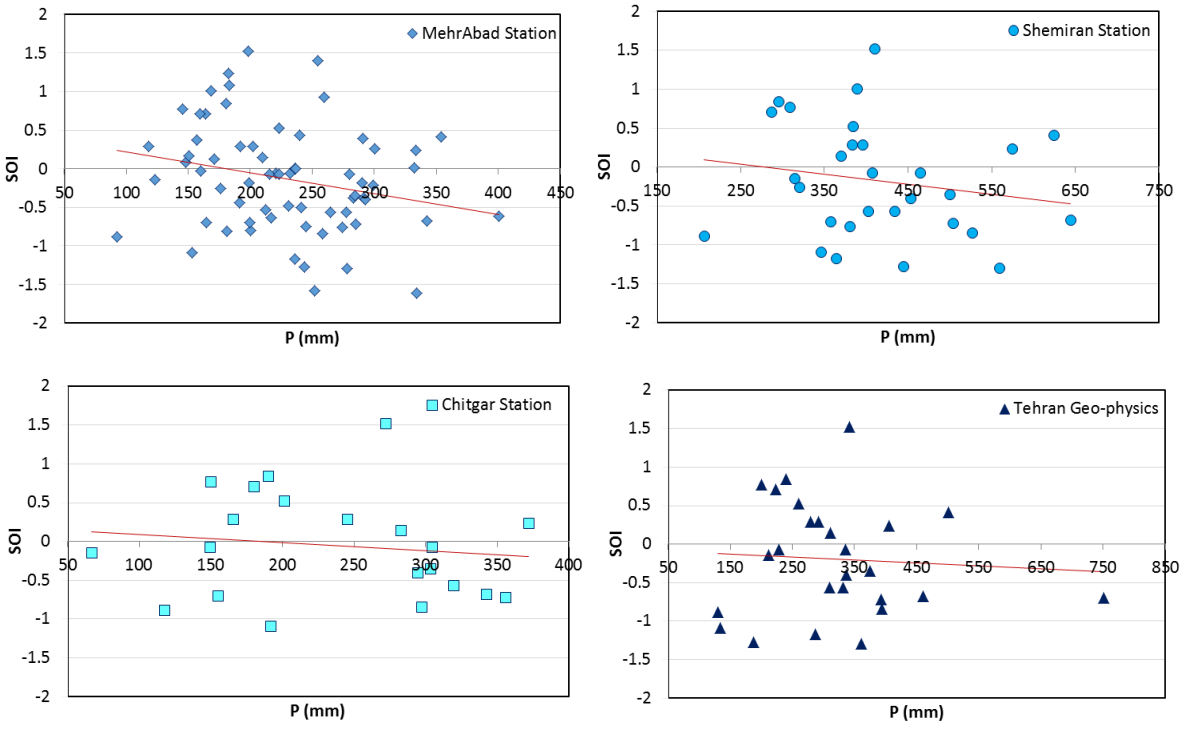

Figure 2: Annual rainfall against SOI index in the station of a) Mehrabad, b) Shemiran, c) Chitgar and 4) Tehran Geophysics

https://doi.org/10.5194/nhess-2019-166
Preprint. Discussion started: 1 August 2019

Natural Hazards and Earth System Sciences
Discussions

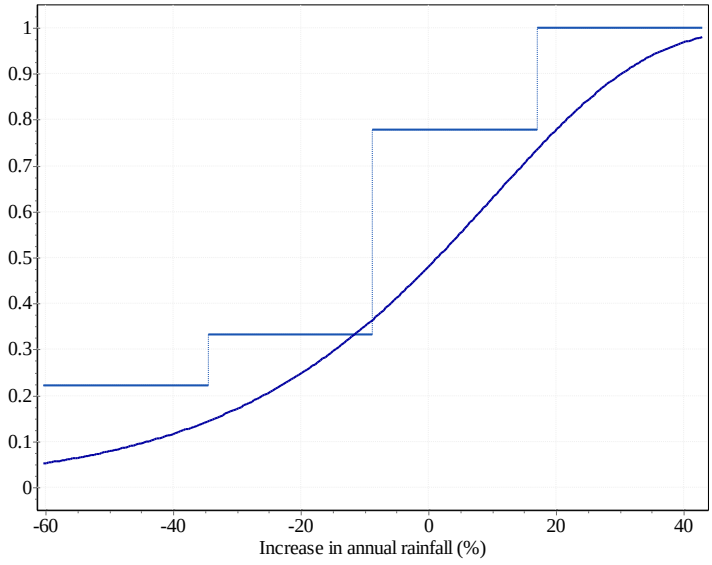

Figure 3: Gumbel Cumulative distribution function fitted on the annual increased percentiles of rainfall

https://doi.org/10.5194/nhess-2019-166
Preprint. Discussion started: 1 August 2019

Natural Hazards and Earth System Sciences
Discussions

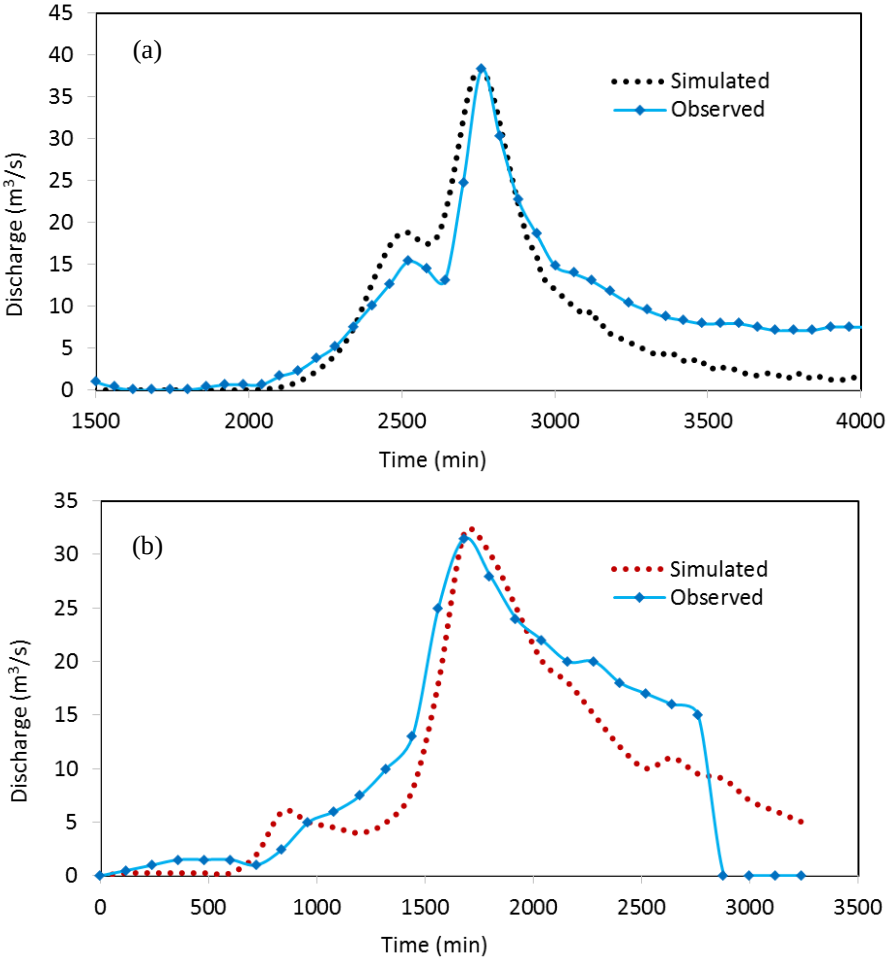

Figure 4: The observed and simulated flood hydrographs at Sulaghan Station in a) calibration step (15–18 April 2003) and b) verification step (16–19 April 2002)

https://doi.org/10.5194/nhess-2019-166
Preprint. Discussion started: 1 August 2019

Natural Hazards and Earth System Sciences
Discussions

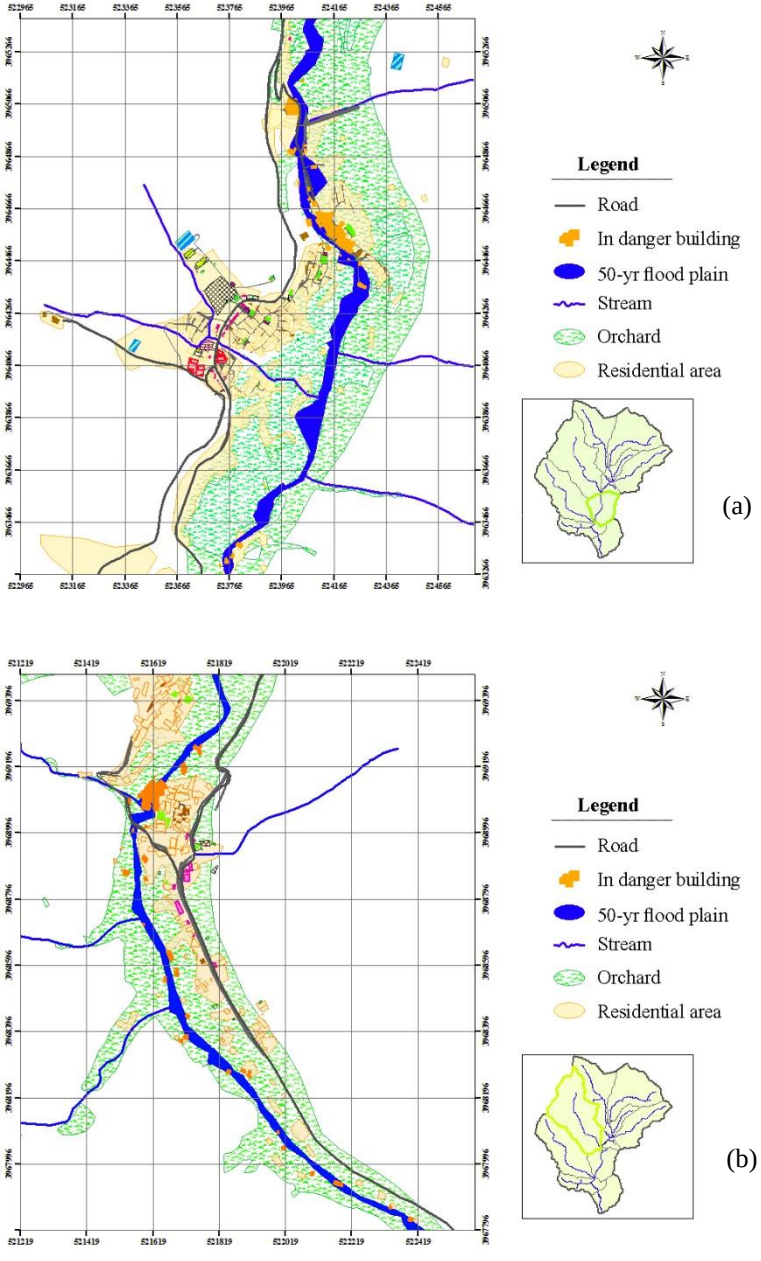

Figure 5: The 50yr floodplain in the sub-basins of a) Sulaghan and b) Sangan